Morphodynamics of barchan-barchan interactions investigated at the grain scale

W. R. Assis[1], E. M. Franklin[1]

[1]School of Mechanical Engineering, UNICAMP - University of Campinas,
Rua Mendeleyev, 200, Campinas, SP, Brazil

Key Points:

- We determine the trajectories of individual grains during barchan-barchan interactions
- We show the origin and destination of moving grains and typical lengths and velocities
- We find the spreading rate of grains over the target barchan once dune-dune collision has occurred

Corresponding author: Erick M. Franklin, `erick.franklin@unicamp.br`

Abstract

Corridors of size-selected crescent-shaped dunes, known as barchans, are commonly found in water, air, and other planetary environments. The growth of barchans results from the interplay between a fluid flow and a granular bed, but their size regulation involves intricate exchanges between different barchans within a field. One size-regulating mechanism is the binary interaction between nearby dunes, when two dunes exchange mass via the near flow field or by direct contact (collision). In a recent Letter (Assis & Franklin, 2020), we identified five different patterns arising from binary interactions of subaqueous barchans, and proposed classification maps. In this paper, we further inquire into binary exchanges by investigating the motion of individual grains while barchans interact with each other. The experiments were conducted in a water channel where the evolution of pairs of barchans in both aligned and off-centered configurations was recorded by conventional and high-speed cameras. Based on image processing, we obtained the morphology of dunes and motion of grains for all interaction patterns. We present the trajectories of individual grains, from which we show the origin and destination of moving grains, their typical lengths and velocities, and flux balances for some barchans. We also show that grains from the impacting dune spread with a diffusion-like component over the target barchan, and we propose a diffusion length. Our results provide new insights into the size-regulating mechanisms of barchans and barcanoid forms found on Earth and other planets.

Plain Language Summary

Barchans are dunes of crescentic shape that are commonly found on Earth, Mars and other celestial bodies. Although of similar shape, their scales vary with the environment they are in, going from the millennium and kilometer for Martian barchans, down to the minute and centimeter in the aquatic case, passing by hundreds of meters and years for aeolian barchans. Other common characteristic is that barchans are organized in dune fields, where barchan-barchan collisions are an important mechanism for their size regulation. We took advantage of the smaller and faster scales of subaqueous dunes and performed experiments in a water channel, which allowed us to determine the trajectories of individual grains while two barchans interacted with each other, something unfeasible from field measurements on terrestrial or Martian deserts. We show typical lengths and velocities of individual grains, and that, in case of barchan collisions, grains from the impacting barchan spread with a diffusive component over the other barchan. Our results provide new insights into the evolution of barchans found in water, air, and other planetary environments.

1 Introduction

Fields of barchan dunes, crescent-shaped dunes with horns pointing downstream, are commonly found in different environments, such as rivers, Earth's deserts and on the surface of Mars (Bagnold, 1941; Herrmann & Sauermann, 2000; Hersen, 2004; Elbelrhiti et al., 2005; Claudin & Andreotti, 2006; Parteli & Herrmann, 2007), being characterized by corridors of size-selected barchans. The growth of dunes results from the interplay between a fluid flow and a granular bed, with sand being transported as a moving layer called bedload. Barchan dunes usually appear under a one-directional fluid flow and limited sand supply (Bagnold, 1941), but the regulation of their size involves intricate interactions between different barchans within a field (Hersen et al., 2004; Hersen & Douady, 2005; Kocurek et al., 2010; Génois, Hersen, et al., 2013; Génois, du Pont, et al., 2013). Barchan-barchan collisions were shown to be an important type of interaction for size regulation (Hersen et al., 2004; Hersen & Douady, 2005), consisting in a fundamental mechanism for sand distribution from large to small barchans. Barchan fields observed in nature result thus from complex interactions between a fluid flow, a sand bed, and existing bedforms.

The first studies on barchan collisions were based on field measurements of aeolian barchans, such as done by Norris and Norris (1961) and Gay (1999). Field measurements are still important in investigating barchan interactions (Vermeesch, 2011; Hugenholtz & Barchyn, 2012), having shown that size regulation and the appearance of barcanoid forms are highly influenced by barchan-barchan collisions. However, given the long timescales in the aeolian case (of the order of the decade), time series for barchan collisions in aeolian fields are frequently incomplete, and conclusive results would need around a century to be achieved. In order to overcome this problem, numerical investigations were conducted using simplified models, both continuum (Schwämmle & Herrmann, 2003; Durán et al., 2005; Zhou et al., 2019) and discrete (Katsuki et al., 2011). Although those investigations reproduced some collision types, model simplifications prevented them from reproducing correctly all existing short-range interactions and collision patterns. Another way to overcome time series limitations is by using water flumes and tanks to investigate barchan collisions, such as done by Endo et al. (2004) and Hersen and Douady (2005). Given the relatively fast scales of the subaqueous case (of the order of the minute), Endo et al. (2004) and Hersen and Douady (2005) obtained complete time series for barchan collisions, describing their dynamics and identifying some of their patterns.

Based on simulations using a continuum model and a stability analysis, Hersen et al. (2004) showed that an isolated barchan within a dune field is marginally stable, since it receives and loses sand in proportion to its width and size of horns, respectively, meaning that the net flux of sand is positive for large barchans and negative for small ones. Therefore, there exists a stable size for an isolated barchan within a dune field, the barchan tending to grow or shrink once the stable size is disturbed. In addition, because smaller dunes move faster than larger ones (Bagnold, 1941), Hersen et al. (2004) argued that barchans should collide and lead to a coarsening of the barchan field. Consequently, they proposed that some mechanism must be responsible for the size regulation of barchans, and suggested that it could be their collision, something that was afterward shown by Hersen and Douady (2005).

Durán et al. (2009) studied the collision of barchans based on numerical simulations and aerial photographs of dune fields in the Western Sahara. The simulations were performed using a continuum model (Kroy et al., 2002b, 2002a; Schwämmle & Herrmann, 2005) to investigate the outcome of barchan-barchan collisions, and the aerial photographs were used for measuring the barchan dimensions and inter-dune space within the fields. Durán et al. (2009) then proposed an equation for the size distribution of barchans based on a balance of sand flux and a collision model, and showed that collisions are important for regulating dune size and inter-barchan spacing. Génois, du Pont, et al. (2013) also proposed a simplified model based on the balance of sand fluxes and elementary rules for barchan-barchan collisions that was used to investigate the origin of corridors with size-selected barchans. The authors performed computations in which they adjusted sand fluxes received and lost by dunes, and, according to the balance between sand fluxes and barchan collisions, obtained corridors of sparse and large or dense and small barchans. As a result, they showed that sand distribution due to collisions is a mechanism that explains the existence of corridors of size-selected barchans. Bo and Zheng (2013) simulated numerically the growth and evolution of a barchan field using a scale-coupled model (Zheng et al., 2009) in order to obtain the probability of barchan-barchan collisions. They found the probabilities for the occurrence of three collision patterns (merging, exchange and fragmentation-exchange, described next), and showed that probabilities vary with the flow strength, grain diameter, grain supply and height ratio of barchans. However, although varying several parameters, the authors did not investigate the mechanics of collisions.

In regard to experiments, subaqueous barchan-barchan collisions were investigated by Endo et al. (2004), Hersen and Douady (2005) and Assis and Franklin (2020). Endo et al. (2004) used a water flume to study the collisions of aligned barchans for different mass ratios, keeping the water flow rate, initial conditions and grain types fixed. They identified three types of collision patterns, which they named absorption, ejection and split, and which we call merging, exchange and fragmentation-chasing (Assis & Franklin, 2020) and explain in what follows. Hersen and Douady (2005) used a water tank in which the motion of a tray created a relative flow between the water and the bedform. They investigated experimentally the collisions of off-centered barchans for different transverse distances of centroids of colliding dunes (referred to as impact or offset parameter), maintaining the mass ratio of barchans, grain type and fluid flow fixed. Based on the experimental results and a stability analysis, Hersen and Douady (2005) showed that barchan collisions produce smaller dunes, being indeed an important mechanism for size-regulation in barchan corridors.

As two barchans approach each other, disturbances in the fluid flow, mainly on the downstream barchan, are expected to affect greatly bedload and surface erosion. Palmer et al. (2012) investigated experimentally the flow disturbances caused by an upstream barchan upon a downstream one when they are in an aligned configuration. The experiments were conducted in a wind tunnel by using model barchans with two different volume ratios (1.0 and 0.175) and fixed longitudinal separation, and the fluid flow was measured at the vertical symmetry plane (aligned in the longitudinal direction) with particle image velocimetry (PIV). They found that the fluid flow on the stoss side of the downstream barchan is highly influenced by the upstream dune, presenting strong turbulent structures which the authors propose to be produced by the interaction between shear layers of both dunes. Those strong turbulent structures would imply stronger bedload over the downstream barchan. Bristow et al. (2018), Bristow et al. (2019) and Bristow et al. (2020) investigated experimentally the flow disturbances caused by a pair of barchans in off-centered configuration in a water channel. For that, they made use of a refractive-index-matching technique together with PIV, so that flow measurements were made at different planes crossing the barchans. They placed pairs of model barchans with a fixed volume ratio (0.125) at different longitudinal distances, and the shape of the downstream barchan was made asymmetric as their separation decreased, in accordance with the results of Hersen and Douady (2005). They showed that the wake of the upstream dune increases turbulence levels on the downstream stoss surface, causing thus a larger erosion on the downstream dune, and that the transverse offset creates a channeling effect around one of the horns of the downstream barchan, promoting dune asymmetry. They showed also that near-bed fluctuations are particularly increased at the reattachment point and that streamwise vortices emerge from the horns, which can enhance even more erosion on the downstream barchan depending on the relative positions of dunes.

1.1 Prior work

In a recent paper (Assis & Franklin, 2020), we investigated experimentally the short-range binary interactions of subaqueous barchans, including collisions, in both aligned and off-centered configurations. The experiments were conducted in a transparent channel where controlled grains were entrained by the water flow, forming a pair of barchans that interacted with each other. We varied the water flow rates, grain types (diameter, density and roundness), pile masses, longitudinal and transverse distances, and initial conditions. As a result, we identified five interaction patterns for both aligned and off-centered configurations and proposed two maps that provide a comprehensive classification for barchan-barchan interactions based on the ratio between the number of grains of each dune, Shields number and alignment of barchans. The five different patterns observed were classified as (i) chasing, when the upstream barchan does not reach the downstream one; (ii) merging, when the upstream barchan reaches the downstream one and they merge; (iii) exchange, when, once the upstream barchan reaches the downstream one, a small barchan is ejected; (iv) fragmentation-chasing, when the downstream dune splits before being reached by the upstream barchan and the new dunes outrun the upstream one; and (v) fragmentation-exchange, when fragmentation initiates, the upstream barchan reaches the splitting dune, and, once they touch, a small barchan is ejected. In addition, we showed that an ejected barchan has roughly the same mass of the impacting one and that the asymmetry of the downstream barchan is larger in wake-dominated processes.

1.2 This study

Although previous studies have shown that barchan-barchan collision is a size-regulating mechanism and identified the interaction patterns, none of them investigated the mass transfers between barchans prior and during collisions, the motion of grains once collision took place, nor, with the exception, partially, of Assis and Franklin (2020), the dune morphodynamics during collisions. In this paper, we further inquire into barchan-barchan interactions by investigating the motion of grains while barchans interact with each other. The experiments were conducted in a water channel where the evolution of pairs of barchans in both aligned and off-centered configurations was recorded by conventional and high-speed cameras. Based on image processing, we tracked bedforms and grains for all interaction patterns. We present the trajectories of individual grains during different stages of barchan-barchan interactions, from which we find the origin and destination of moving grains, their typical lengths and velocities, and flux balances for some barchans. We also show that grains from the impacting dune spread with a diffusion-like component over the target barchan, and propose a diffusion length for their dispersion. The present results provide new insights into the shape and size variations of barchans and barcanoid forms found in water, air, and other planetary environments.

In the following, Sec. 2 describes the experimental setup and procedure, Sec. 3 presents the obtained results, and Sec. 4 presents the conclusions.

2 Experimental Setup

The experimental device is the same as in Assis and Franklin (2020), consisting of a water reservoir, two centrifugal pumps, a flow straightener, a 5-m-long closed-conduit channel, a settling tank, and a return line, where a pressure-driven water flow was imposed in the order just described. The channel was made of transparent material and had a rectangular cross section 160 mm wide and $2\delta = 50$ mm high, its 1-m-long test section starting 3 m downstream of the channel inlet. This corresponds to 40 hydraulic diameters, which assured a developed channel flow upstream the bedforms. The remaining 1-m-long section connected the exit of the test section to the settling tank. Figures 1d and 1a present, respectively, the layout of the experimental device and a photograph of the test section.

Controlled grains were poured inside the channel, filled previously with water, forming two conical piles that were afterward deformed into barchans by the imposed water flow. The pairs of bedforms were formed in either aligned or off-centered configurations and the longitudinal distance between initial piles was of the order of the diameter of the upstream pile. The size of the upstream dune (impact dune) was always equal or lesser than that of the downstream dune (target dune), since the dune velocity varies inversely with its size (Bagnold, 1941), their mass ratio varying within 0.021 and 1. With that procedure, we obtained binary interactions for all five patterns described in Assis and Franklin (2020), in both aligned and off-centered configurations.

The ensemble of tests used tap water at temperatures within 25 and 28 °C and round glass beads ($\rho_s = 2500$ kg/m^3) with diameters 0.15 mm $\leq d_s \leq$ 0.25 mm and 0.40 mm $\leq d_s \leq$ 0.60 mm (not mixed with each other). In the following, we consider d as the

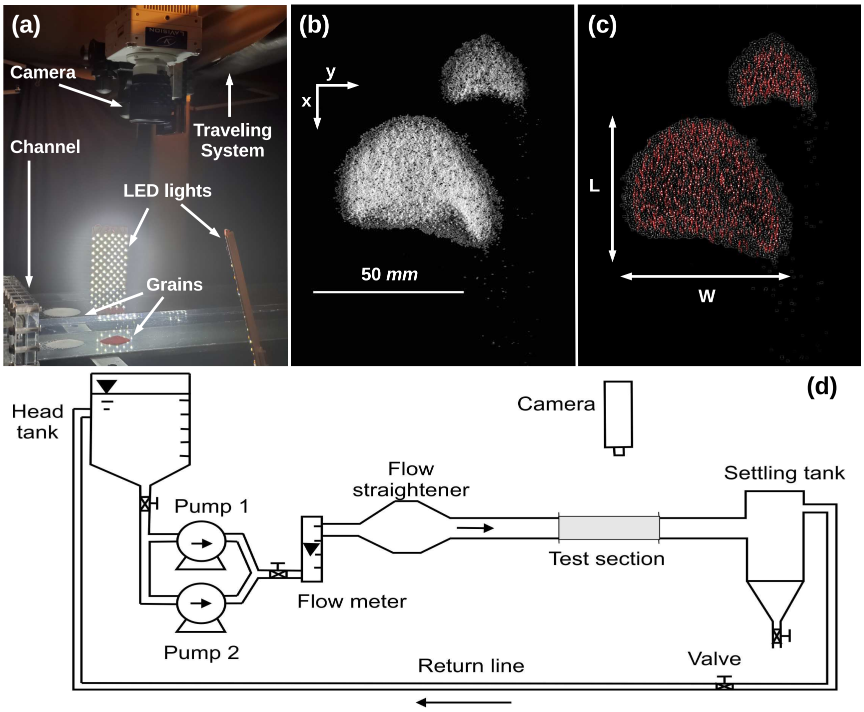

Figure 1. Experimental setup, barchans and grains detection, and definition of some geometrical parameters. (a) Photograph of the experimental setup showing the test section, camera, traveling system, LED lights, and dunes on the bottom wall of the channel. (b) Top-view image of two interacting barchans, the water flow is from top to bottom. (c) Binarized image of interacting barchans showing identified grains that were tracked along images and some of the barchan dimensions. (d) Layout of the experimental setup.

mean value of d_s. In order to facilitate the tracking of grains, tests focused on the mass exchange between barchans used 96-98 % of white grains and 4-2 % of black grains, for both dunes, and tests focused on particle diffusion at the grain scale used white grains for the impact and red grains for the target dune (colors inverted with respect to Assis and Franklin (2020)), all of them with the same density, diameter and roundness for a given test. The cross-sectional mean velocity of water, U, was fixed at either 0.243 or 0.278 m/s, corresponding to Reynolds numbers based on the channel height, Re $= \rho U 2\delta/\mu$, of 1.22×10^4 and 1.39×10^4, respectively, where μ is the dynamic viscosity and ρ the density of the fluid. The shear velocities on the channel walls in the absence of dunes, u_*, were computed based on measurements with a two-dimensional two-component particle image velocimetry (2D2C-PIV) device and found to follow the Blasius correlation (Schlichting, 2000), being 0.0141 and 0.0159 m/s for the two imposed water flows. By considering the fluid velocities applied to each grain type, the Shields number, $\theta = (\rho u_*^2)/((\rho_s - \rho)gd)$, varied within 0.027 and 0.086, where g is the acceleration of gravity. Because the shear velocity varies over the surface of each dune, as well as in some regions on the channel walls when in the presence of barchans (Bristow et al., 2018, 2019, 2020), we use u_* (undisturbed by dunes) as the reference value for the fluid shearing. Microscopy images of the used grains and a table summarizing the tested conditions are available in the supporting information.

The evolution of bedforms was recorded by either a high-speed or a conventional camera mounted on a traveling system and placed above the channel, both the camera and traveling system being controlled by a computer. The high-speed camera was of complementary metal-oxide-semiconductor (CMOS) type with maximum resolution of 2560 px $\times$ 1600 px at 800 Hz, and we set its region of interest (ROI) within 2176 px $\times$ 960 px and 2560 px $\times$ 1600 px and the frequency to 200 Hz. The field of view varied from 117 mm $\times$ 75 mm to 205 mm $\times$ 112 mm, the area covered by each grain varying within 6 to 32 px in the images. The conventional camera, also of of CMOS type, had a maximum resolution of 1920 px $\times$ 1080 px at 60 Hz, which were the ROI and frequency set in the tests. For the tests on the exchange pattern, the field of view was 160 mm $\times$ 90 mm, the area covered by each grain (d = 0.2 mm) corresponding thus to approximately 5 px, while the tests on the merging pattern had a field of view of 260 mm $\times$ 146 mm, the area covered by each grain (d = 0.5 mm) corresponding to approximately 11 px. We mounted lenses of 60 mm focal distance and F2.8 maximum aperture on the cameras and made use of lamps of light-emitting diode (LED) branched to a continuous-current source to provide the necessary light while preventing beating with the cameras. The conversion from px to a physical system of units was made by means of a scale placed in the channel previously filled with water. Movies showing the motion of grains over approaching and colliding barchans are available in the supporting information.

The acquired images were processed by numerical scripts written in the course of this work and based on Crocker and Grier (1996), Kelley and Ouellette (2011), Houssais et al. (2015) and Cúñez and Franklin (2020). They basically removed the image background, binarized the images, identified the barchan morphology and individual grains, and computed the main morphological properties of bedforms, their relative distances and the motion of grains. Figures 1b and 1c present, respectively, raw and processed images, the latter showing identified grains that were tracked along images.

Given its high frequencies, the high-speed camera uses an internal memory to store the acquired images, to be discharged to a computer once the measurements are over or the memory full. Depending on the tests, the time for discharging image files was greater than that for reaching the next stage of interaction between dunes. These were the cases of tests with higher velocities (U = 0.278 m/s), for which once the images were discharged we had to restart the tests from the beginning, under the same conditions, until reaching the next stage to be recorded. For the other tests, measurements were made in a continuous mode, the camera having discharged the files to the computer before the next stage was reached.

3 Results and discussion

In Assis and Franklin (2020), we identified five different patterns as resulting from the short-range interaction for both aligned and off-centered configurations. We present now experimental data at the grain scale that would be difficult to obtain from field measurements, such as the trajectories of individual grains, the exchange of grains between barchans, typical lengths and velocities, and the spreading of grains after collision has taken place. Because in Assis and Franklin (2020) the ensemble of tests for each pattern showed the same behavior, we present next the motion of grains for one instance of each pattern, in both aligned and off-centered configurations.

3.1 Trajectories of grains leaving dunes and mass exchange

We tracked moving grains during the interaction of barchans, and computed their trajectories. The trajectories of grains migrating from one dune to another, and also of grains leaving dunes and being entrained further downstream by the fluid, are of particular interest. Those trajectories reveal not only the masses exchanged between nearby dunes and lost by the entire system, but also details on how these exchanges and losses occur. Figures 2 to 6 show the trajectories of grains during different stages of barchan-barchan interactions, for all the five patterns in both aligned and off-centered configurations. Figures 2 to 6 correspond to the chasing, merging, exchange, fragmentation-chasing and fragmentation-exchange patterns (Assis & Franklin, 2020), respectively, where subfigures on the top are related to aligned and on the bottom to off-centered cases. Red lines correspond to grains leaving the upstream (impact) dune, blue lines to grains leaving the downstream (target) dune, white lines to grains migrating from a downstream bedform to the upstream one, and magenta lines to grains leaving a new bedform. For the sake of clarity, the trajectories of a small portion of grains are plotted in Figures 2 to 6 (in average, 45% of trajectories that took place during approximately 9 s were plotted, but percentages vary from 5% to 100% depending on the case).

For the chasing pattern, the wake of the upstream barchan strongly affects the downstream one (Bristow et al., 2018, 2019, 2020), the downstream barchan being strongly eroded and, due to small asymmetries, becoming eventually off-centered even in the aligned case. We observe a strong number of grains leaving the downstream barchan (in the aligned case, once dunes become off-centered), and the asymmetry of horns increases due to grains received asymmetrically from the upstream barchan. With both cases being eventually in an off-centered configuration, only grains from one of the horns of the upstream barchan reach the downstream one, and part of them simply go around the downstream barchan. At that stage (Figures 2b and 2d), we measured that approximately 25% of grains leaving the upstream barchan go over the downstream dune (24% in the aligned and 28% in the off-centered case), and that 7% go around it and 69% are directly entrained further downstream in the aligned case, while 44% go around the downstream barchan and 28% are directly entrained further downstream in the off-centered case. In addition, we computed the difference between grains received and lost by the downstream barchan (still at the late stage) and found that it reaches deficits of 18% and 33% in the aligned and off-centered cases, respectively. The measured deficits corroborate the size decrease of the downstream barchan in the chasing pattern.

For the merging pattern, we observe some differences between the aligned and off-centered cases. At the initial stage of the aligned case, a great part of grains leaving the upstream dune reaches the downstream one (92% of grains are incorporated by the downstream bedform), deforming the downstream barchan into a barcanoid form. At a later

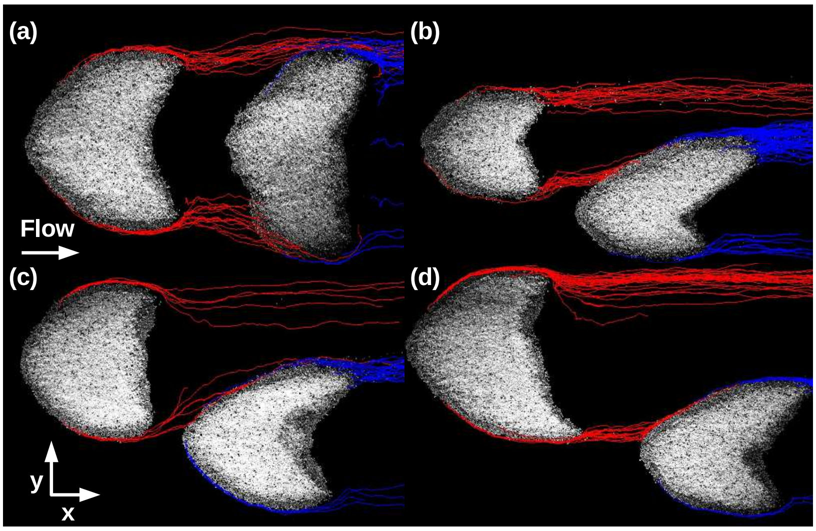

Figure 2. Trajectories of some grains at two different intervals for the chasing pattern. Figures (a) and (b) correspond to two different stages of the interaction for the aligned case, and figures (c) and (d) to two different stages for the off-centered case. Red lines correspond to grains leaving the upstream dune and blue lines to grains leaving the downstream one.

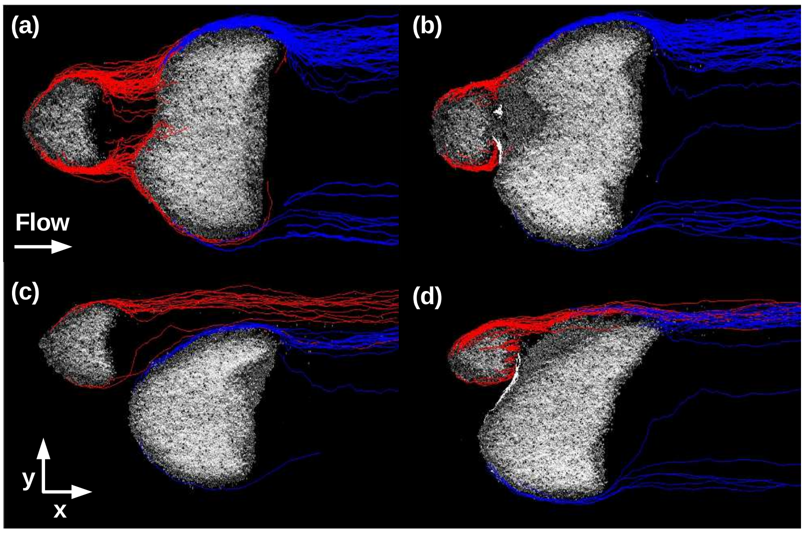

Figure 3. Trajectories of some grains at two different intervals for the merging pattern. Figures (a) and (b) correspond to two different stages of the interaction for the aligned case, and figures (c) and (d) to two different stages for the off-centered case. Red lines correspond to grains leaving the upstream dune, blue lines to grains leaving the downstream one, and white lines to grains migrating from the downstream bedform to the upstream one.

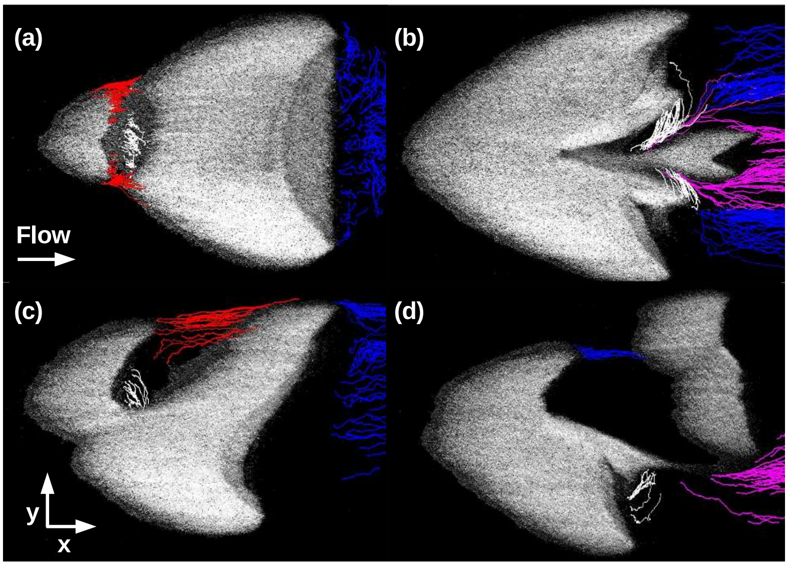

Figure 4. Trajectories of some grains at two different intervals for the exchange pattern. Figures (a) and (b) correspond to two different stages of the interaction for the aligned case, and figures (c) and (d) to two different stages for the off-centered case. Red lines correspond to grains leaving the upstream dune, blue lines to grains leaving the downstream one, white lines to grains migrating from the downstream bedform to the upstream one, and magenta lines to grains leaving the new bedform.

stage, when dunes are almost colliding, the recirculation region in the wake of the upstream barchan carries grains from the downstream bedform to the upstream one, eroding the toe of the downstream bedform and forming a monolayer carpet between dunes before merging occurs. In the off-centered case, the main differences are that a much smaller number of grains leaving the upstream dune at the initial stage reaches the downstream one (only 1% of them), and that, before merging occurs, the recirculation region of the upstream barchan does not strongly erode the leading edge of the downstream dune, forming only the monolayer carpet.

During the initial stages, the behaviors of the exchange pattern in aligned and off-centered configurations (Figures 4a and 4c) are similar to those of the merging pattern (Figures 3a and 3c). However, after collision has taken place, the perturbation caused by the impacting barchan leads the resulting bedform to eject a new barchan. Along this text, we refer sometimes to the resulting (merged) and ejected bedforms as *parent* and *baby* barchans, respectively. In the aligned case, the new barchan is ejected from a central position at the lee face, and we observe that a considerable part of grains migrate from the new ejected barchan toward the upstream bedform (22% of the grains that leave the new barchan), forming two branches connecting, during a certain period, both dunes. In the off-centered case, the new barchan is ejected from one of the horns, and grains do not migrate from the ejected barchan toward the upstream dune. Instead, the ejected barchan continues receiving grains from the upstream dune.

In the fragmentation-chasing pattern, the perturbation caused by the wake of the upstream barchan is so strong that it splits the downstream dune into two smaller barchans. In both the aligned and off-centered cases, the downstream dune receives grains from the upstream barchan, but loses a larger quantity of grains (reaching deficits of 64% and 19%

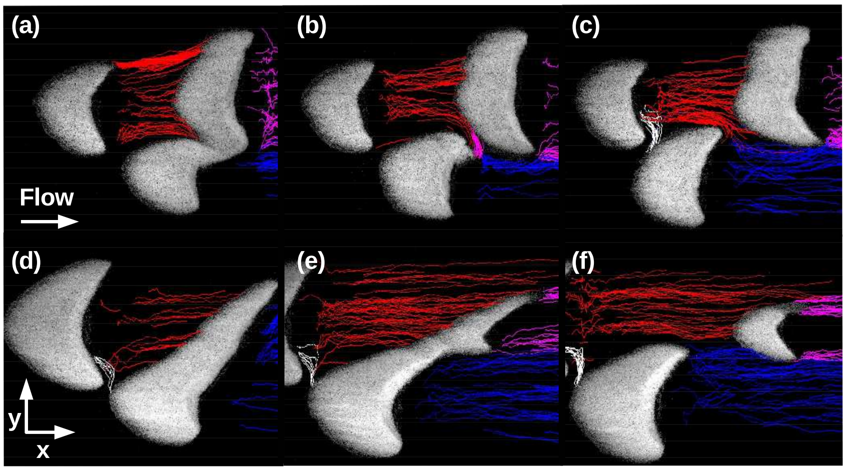

Figure 5. Trajectories of some grains at three different intervals for the fragmentation-chasing pattern. Figures (a), (b) and (c) correspond to three different stages of the interaction for the aligned case, and figures (d), (e) and (f) to three different stages for the off-centered case. Red lines correspond to grains leaving the upstream dune, blue lines to grains leaving the downstream one, white lines to grains migrating from the downstream bedform to the upstream one, and magenta lines to grains leaving a new bedform.

in the aligned and off-centered cases, respectively). Once divided, the new barchans travel faster than the upstream one and they do not collide. However, one of the new barchans remains for some time close to the upstream one and some of its grains migrate toward the latter, entrained by the recirculation region.

The fragmentation-exchange pattern is roughly similar to the fragmentation-chasing one, the main difference being that the impact barchan collides with one of the split bedforms. During the collision process, some grains are entrained from the downstream dune toward the impact barchan by the wake of the latter. Around 45% of the grains leaving the downstream bedforms migrate to the impact barchan in the aligned case (46% and 42% in Figures 6a and 6b, respectively), while the percentages are 70% and 5% for the two stages of the off-centered case shown in Figures 6c and 6d, respectively. In the aligned case these percentages consider both split bedforms, while those for the off-centered case consider only grains from the split bedform closer to the impact barchan. The high percentage found in the approaching of barchans in the off-centered case (Figure 6c) reflects the formation of a granular bridge between them, which, once formed, unite both barchans with the consequent decrease in grains entrained toward the upstream dune (Figure 6d).

A table summarizing the percentages of grains exchanged between dunes is available in the supporting information.

3.2 Lengths and velocities of exchanged grains

Based on grain trajectories, we identified, for the characteristic routes distinguished in Subsection 3.1, typical lengths and velocities of grains migrating from one dune to an-

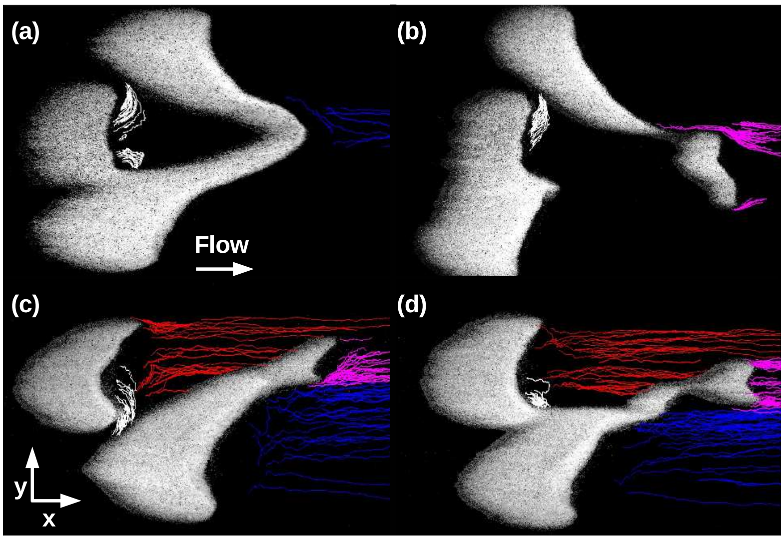

Figure 6. Trajectories of some grains at two different intervals for the fragmentation-exchange pattern. Figures (a) and (b) correspond to two different stages of the interaction for the aligned case, and figures (c) and (d) to two different stages for the off-centered case. Red lines correspond to grains leaving the upstream dune, blue lines to grains leaving the downstream one, white lines to grains migrating from the downstream bedform to the upstream one, and magenta lines to grains leaving a new bedform.

other. For that, we computed the displacement lengths in the longitudinal and transverse directions, Δx and Δy, respectively, as well as the time-averaged velocities in the longitudinal and transverse directions, V_x and V_y, respectively, of exchanged particles. Displacements were computed as the total distances traveled by grains from their departure from one dune until reaching another one, and average velocities as the mean values for each grain during its migration. We then plotted their respective probability distribution functions (PDFs), and we present some of them in Figures 7 and 8 (other PDFs are available in the supporting information).

Figures 7a to 7d present PDFs of total distances traveled by grains moving from the impact toward the target barchan for the merging pattern at the begining of the aligned interaction (Figures 7a and 7b) and at the collision instant in the off-centered interaction (Figures 7c and 7d), for both the longitudinal and transverse directions, Δx and Δy, respectively. These distances correspond to the differences between the final and initial positions of each grain, and they are normalized by $L_{drag} = \rho_s \rho^{-1} d$ (Hersen et al., 2002). L_{drag} is a length scale of inertial nature proposed by Hersen et al. (2002), and it is proportional to the saturation length, which is the typical distance for the sand flux to reach equilibrium with a varying fluid flow (Andreotti et al., 2002; Charru et al., 2013). For the beginning of the aligned case (trajectories shown in Figure 3a), Δy presents a roughly symmetric distribution with two peaks close to a zero mean and Δx presents higher values when compared with the collision instant of the off-centered case, showing that traveled lengths are proportional to the separation distances between dunes. In the off-centered case at the collision instant (trajectories shown in Figure 3d), Δy presents a most probable value of approximately zero, and a skewness toward positive values, which is a consequence of the off-centered condition. From the PDFs, we obtain mean values of $\Delta x/L_{drag}$ = 33.4 and $\Delta y/L_{drag}$ = 2.4, with standard deviations of, respectively, 18.2 and 6.7L_{drag}

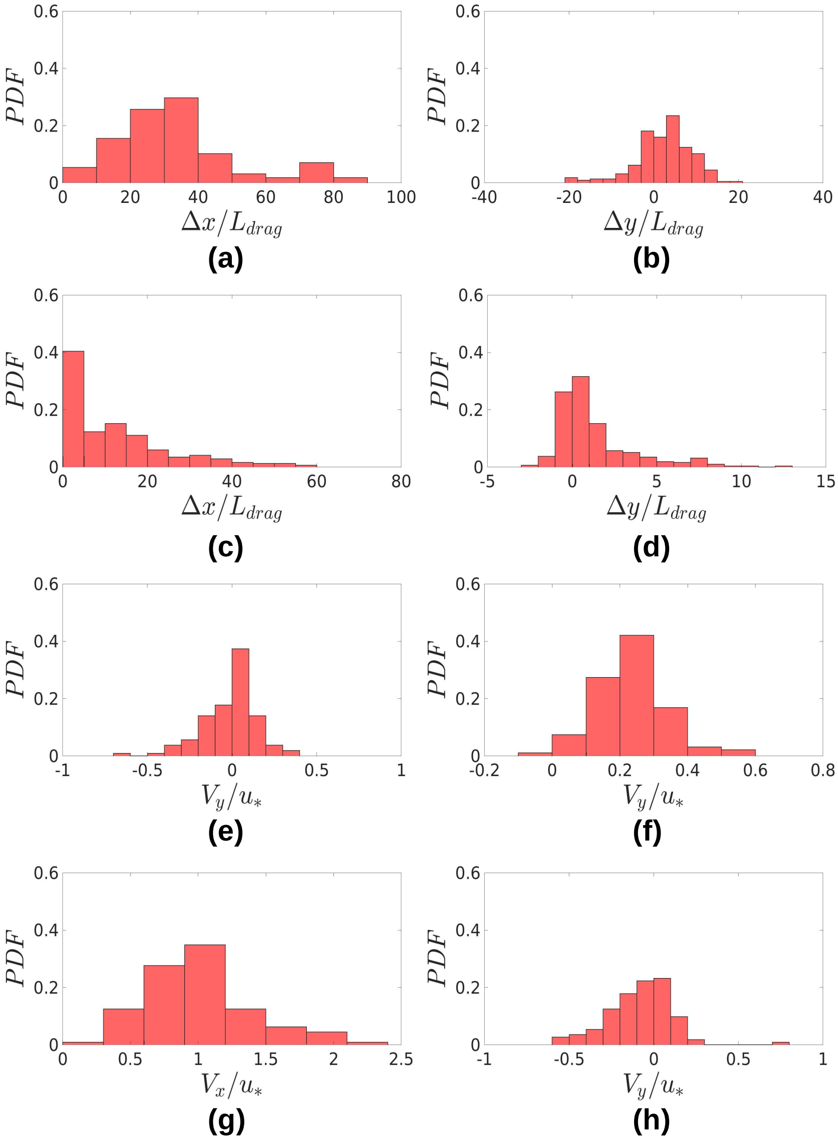

Figure 7. PDFs of total distances traveled by grains in longitudinal and transverse directions, Δx and Δy, respectively, normalized by L_{drag}, and PDFs of time-averaged velocities in the longitudinal and transverse directions, V_x and V_y, respectively, normalized by u_*. Figures (a) and (b) correspond to red trajectories in Figure 3a, Figures (c) and (d) to red trajectories in Figure 3d, Figures (e) and (f) to red trajectories in Figures 2a and 2b, respectively, and Figures (g) and (h) to red trajectories in Figure 5c.

for the beginning of the aligned case, and mean values of $\Delta x/L_{drag}$ = 12.6 and $\Delta y/L_{drag}$ = 1.3, with standard deviations of, respectively, 12.7 and $2.4L_{drag}$ for the off-centered case at the collision instant.

Figures 7e and 7f show PDFs of the transverse velocity V_y of grains migrating from the upstream barchan to the dowstream one in the chasing pattern in the aligned configuration at the two instants shown in Figures 2a and 2b, respectively. We observe that, while the PDF of 7e has positive and negative values, being roughly symmetric around a zero mean, that of Figure 7f has mostly positive values. We obtain, respectively, mean values of V_y/u_* equal to -0.01 and 0.23, with standard deviations of 0.16 and $0.10u_*$. These PDFs reflect the symmetry of the chasing pattern at its initial stage (Figure 2a) and its asymmetric final stage (Figure 2b).

Figures 7g and 7h show PDFs of the time-averaged velocities in the longitudinal and transverse directions, V_x and V_y, respectively, of grains migrating from the upstream barchan toward the target one in the fragmentation-chasing pattern in aligned configuration. These PDFs correspond to the red trajectories from the impact barchan toward one of the split barchans, namely that in a more aligned position, at the instant shown in Figure 5c. PDFs show only positive values for V_x, since grains move downstream, and positive and negative values of V_y around an approximately zero mean. The obtained mean values were V_x/u_* = 1.01 and V_y/u_* = -0.08, and the corresponding standard deviations were 0.39 and $0.19u_*$, respectively. We observe that values for V_x are relatively high, showing that the fluid flow is higher in that region (channeling of the mean flow and perhaps increased fluctuations), with local values of shear velocity greater than the value of reference u_* (Bristow et al., 2018).

The trajectories of grains migrating to an upstream bedform are of particular interest. In the one hand, they accelerate the collision of dunes, as, for example, in the fragmentation-exchange pattern (Figure 6), by generating a bridge between dunes. On the other hand, they modulate the ejection of a new (baby) barchan in the exchange pattern (Figure 4b), by bringing part of grains of the baby barchan back to its parent. In both cases, a granular bridge is transiently formed between the interacting dunes.

Figures 8a and 8b show PDFs of total distances traveled by grains moving from the baby toward the parent barchan for the exchange pattern in aligned configuration, in the longitudinal and transverse directions, Δx and Δy, respectively, and Figures 8c and 8d show the respective PDFs of V_x and V_y. Values are normalized by L_{drag} and u_*, and the PDFs correspond to the white trajectories in Figure 4b. For the displacements, we obtain mean values of $\Delta x/L_{drag}$ = 9.1 and $\Delta y/L_{drag}$ = 8.0, with standard deviations of, respectively, 5.4 and $17.8L_{drag}$. The PDF of Δx shows only one peak, with most of samples as well as the mean average exhibiting positive values. Grains from the ejected barchan move downstream distances of approximately $9L_{drag}$ in average, which is directly proportional to the distance between barchans. On the other hand, the PDF of Δy shows two peaks around the zero value, corresponding to most probable values of approximately $\pm 15L_{drag}$, and a large dispersion around the mean average. This reflects the fact that, by symmetry, grains migrating from the ejected barchan toward its parent travel laterally in opposite directions (positive and negative). We should expect then a zero mean value; however, because Figure 8b corresponds to a single experiment, the obtained value differs from zero. These grains form two transient bridges, one at each side of the barchans, connecting the baby barchan to its parent as the former is ejected. Similar patterns appear for the velocities, with only one peak and most of samples exhibiting positive values for V_x, and two peaks around a zero value for V_y. The obtained mean values are V_x/u_* = 0.55 and V_y/u_* = 0.37, the corresponding standard deviations are 0.31 and $1.13u_*$, respectively, and the most probable values of V_y are approximately $\pm 0.75u_*$. For the off-centered configuration, there are no grains migrating from the baby barchan toward the parent one, as seen in Figure 4d.

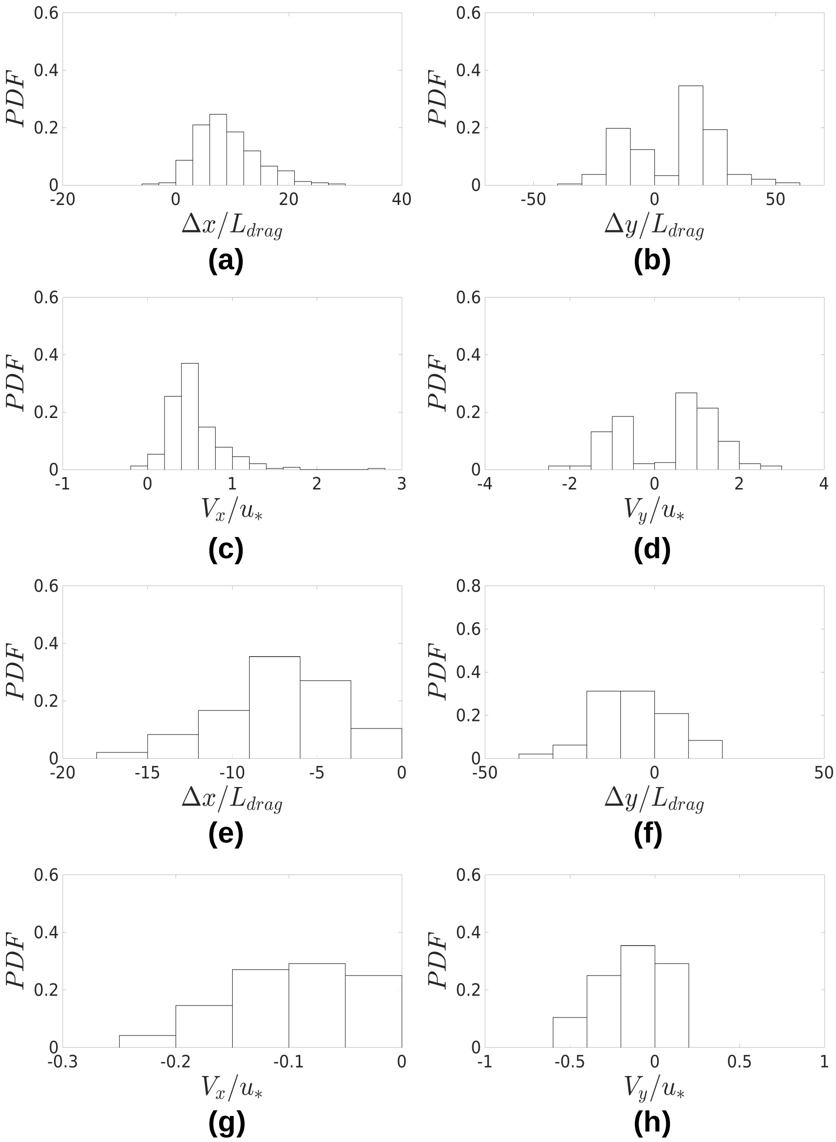

Figure 8. PDFs of total distances traveled by grains in longitudinal and transverse directions, Δx and Δy, respectively, normalized by L_{drag}, and PDFs of time-averaged velocities in the longitudinal and transverse directions, V_x and V_y, respectively, normalized by u_*. Figures (a) to (d) correspond to white trajectories in Figure 4b and Figures (e) to (h) to white trajectories in Figure 6a

Figures 8e and 8f show PDFs of normalized distances traveled by grains moving from the splitting dune toward the impact barchan for the fragmentation-exchange pattern in aligned configuration, in the longitudinal and transverse directions, $\Delta x/L_{drag}$ and $\Delta y/L_{drag}$, respectively, and Figures 8g and 8h show PDFs of the corresponding time-averaged velocities, V_x/u_* and V_y/u_*. Different from the exchange pattern in the aligned case, the barchan ejection occurs asymmetrically and grains do not migrate back to the parent barchan; therefore, we do not present statistics for the grains migrating from the baby barchan, but for a stage before, with grains migrating from the splitting dune. For the displacements, we observe that grains move upstream, with mean values of -7.2 and -6.3 for $\Delta x/L_{drag}$ and $\Delta y/L_{drag}$, respectively, and corresponding standard deviations of 3.5 and $11.4L_{drag}$. Grains migrating from the splitting dune toward the impact barchan present thus negative values for Δx, being entrained upstream. For the transverse displacements, one should expect a symmetric PDF around a mean value equal to zero; however, Figure 8f corresponds to one test run in which asymmetries occurred (given the discrete nature of the problem), and a non-zero mean emerged for Δy. Again, similar patterns appear for V_x and V_y, with mean values of V_x/u_* = -0.10 and V_y/u_* = -0.14, and the corresponding standard deviations of 0.06 and $0.18u_*$, respectively.

In summary, we computed typical displacements and velocities of grains exchanged between interacting barchans, and plotted the corresponding PDFs. In general, mean values of traveled distances in the longitudinal direction are proportional to the longitudinal separation between barchans, while in the transverse direction they are proportional to the transverse offset between bedforms. For the longitudinal component of velocities, mean values are mostly positive but can be negative when grains are entrained by the recirculation region of the upstream dune, which happens in some cases when two bedforms are very close, almost touching each other. In the main, they are one order of magnitude smaller than the undisturbed shear velocity over the channel wall (reference value), u_*, but in some regions where the fluid flow is locally accelerated and/or has its turbulence level increased V_x reaches values of the same order of magnitude of u_*. For the transverse component, mean values tend to zero for aligned bedforms, due to symmetry, and deviate from zero for off-centered bedforms. For some aligned bedfoms, such as the ejection of a baby barchan in the aligned-exchange configuration, distributions of transverse displacements and velocities are bimodal and roughly symmetrical around a zero mean.

Distances and velocities for the remaining cases are similar to those presented in Figures 7 and 8, and some of them are presented in the supporting information.

3.3 Spreading after collision

Having analyzed in Subsections 3.1 and 3.2 the motion of grains between bedforms, we investigate now the motion, after collision has taken place, of grains originally in the impact barchan. For that, we present data at both the barchan and grain scales. At the barchan scale, some of the images obtained by Assis and Franklin (2020) are now further treated for measuring the spreading of the impacting bedform based on the evolution of its area over the target barchan. At the grain scale, we determine, from new movies, typical trajectories of individual grains by tracking their motion once collision has occurred.

By observing the evolution of the impacting bedform after collision has taken place in the merging and exchange cases, we notice two distinct stages in its evolution. The first stage corresponds to a barchan shape being stretched and becoming a longitudinal stripe, while in the second one the stripe widens slowly along time. Both stages can be observed in Figures 9 to 11, which show grains from the impact barchan over the target one, and also in Figure 12, which shows the width of the longitudinal stripe W_d as a function of time, Figure 12a corresponding to the entire collision processes and Figure 12b to the second stage.

For the first stage, Figures 9 and 10 show how grains originally in the impact barchan spread over the target one during merging and exchange processes, respectively, in the aligned case. Red (clear) regions correspond to grains from the impact barchan and white (darker) to grains from the target one, and different instants are shown from top to bottom. Figures 9 and 10 show that, indeed, the impacting bedform, which had initially a barchan shape, is stretched and deformed into a longitudinal stripe in both cases, while its wake disturbs the surface of the target barchan. In the case of the exchange pattern, the perturbation is strong enough to eject a new barchan that does not contain grains from the impact dune.

Figure 11 presents the second stage of the deformation of the impacting bedform, Figures 11a and 11b corresponding to a merging process and Figures 11c and 11d to an exchange process. We observe that the longitudinal stripe widens slowly along time, in what resembles a diffusion process, taking 300 s to widen 0.91 mm in the merging case and 330 s to widen 1.67 mm in the exchange case (values of W_d as a function of time during the second stage are presented in Figure 12b). The corresponding expansion (widening) velocities are, respectively, 3×10^{-6} and 5×10^{-6} m/s, which correspond to 2×10^{-4} and $3 \times 10^{-4} u_*$, while grain velocities are much larger, of the order of $10^{-1} u_*$ (as shown next). Because the main flow is in the longitudinal direction, we conjecture that the widening of the longitudinal stripe is caused by the erratic trajectories of grains, which are, in addition, amplified in the transverse direction due to the lateral slopes of the bedform. Although not a pure diffusion in the strict sense, we describe next this widening processes as a diffusion-like mechanism given the resemblance. In order to investigate that, we followed individual grains during the stripe widening and computed their trajectories, displacement lengths and velocities.

Figures 13a and 13b show some trajectories of grains (from the impact dune) over the target barchan for the merging and exchange processes, respectively. We observe a small transverse component that varies from grain to grain that contributes to the stripe widening. In order to scrutinize their relation, we computed mean values and standard deviations of displacements and velocities for a large amount of particles, obtaining diffusion-like measurements at the grain scale. The considered grains were those from the impact barchan that started moving over the target barchan at positions within a width equivalent to that of the impact dune (boundaries shown in Figure 13).

Figure 14 presents PDFs of total distances traveled by the followed grains in the longitudinal and transverse directions, Δx (Figures 14a and 14c) and Δy (Figures 14b and 14d), respectively. These distances correspond to the differences between the final and initial positions of each grain, and they are normalized by L_{drag}. Figures 14a and 14b correspond to the merging and Figures 14c and 14d to the exchange pattern.

PDFs of $\Delta x/L_{drag}$ (Figures 14a and 14c) show a decreasing distribution that seems exponential, but we prefer to not assert its form for the moment, however, given the relative small size of our samples. Longitudinal distances have average values of approximately 4 and $6L_{drag}$ and RMS (root mean square) averages of 5 and $10L_{drag}$ for the merging and exchange patterns, respectively. Distributions of $\Delta y/L_{drag}$ (Figures 14b and 14d) show a Gaussian-like behavior, peaked close to zero. Here again, we prefer to not assert the form of the distribution. Transverse distances traveled by the followed grains show average values of approximately 0.1 and -$0.2L_{drag}$, standard deviations of 0.8 and $1.5L_{drag}$, and RMS averages of 0.8 and $1.5L_{drag}$. These values show ensemble averages around zero with large dispersions, indicating that grains travel longitudinally with considerable deviations in the transverse direction that are symmetrical with respect to the longitudinal direction. This kind of trajectory spreads the longitudinal stripe in a way that resembles a diffusion mechanism.

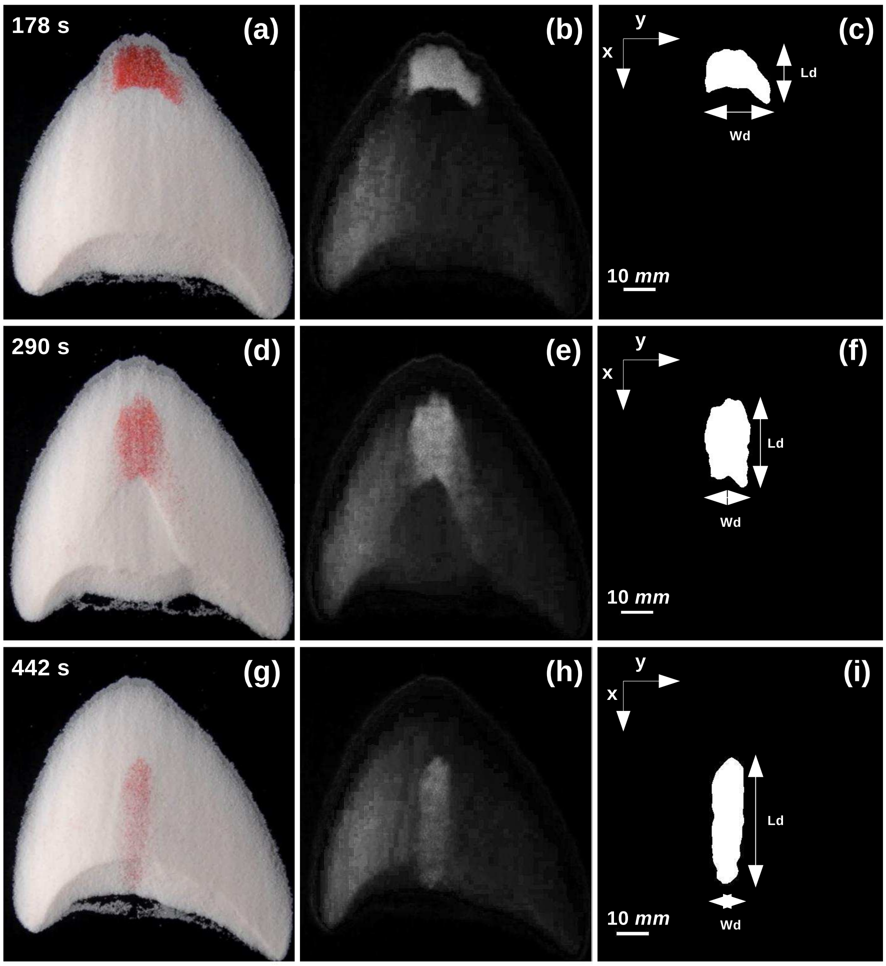

Figure 9. Distribution of grains from the impact barchan over the target one during a merging process in the aligned case. Red (clear in figures b, e and h) grains come from the impact barchan and white (darker in figures b, e and h) grains are from the target one. From top to bottom, figures correspond to different instants (shown in figures), and from left to right figures correspond to raw, grayscale and binary images. L_d is the length and W_d the width of the structure formed with grains from the impact barchan.

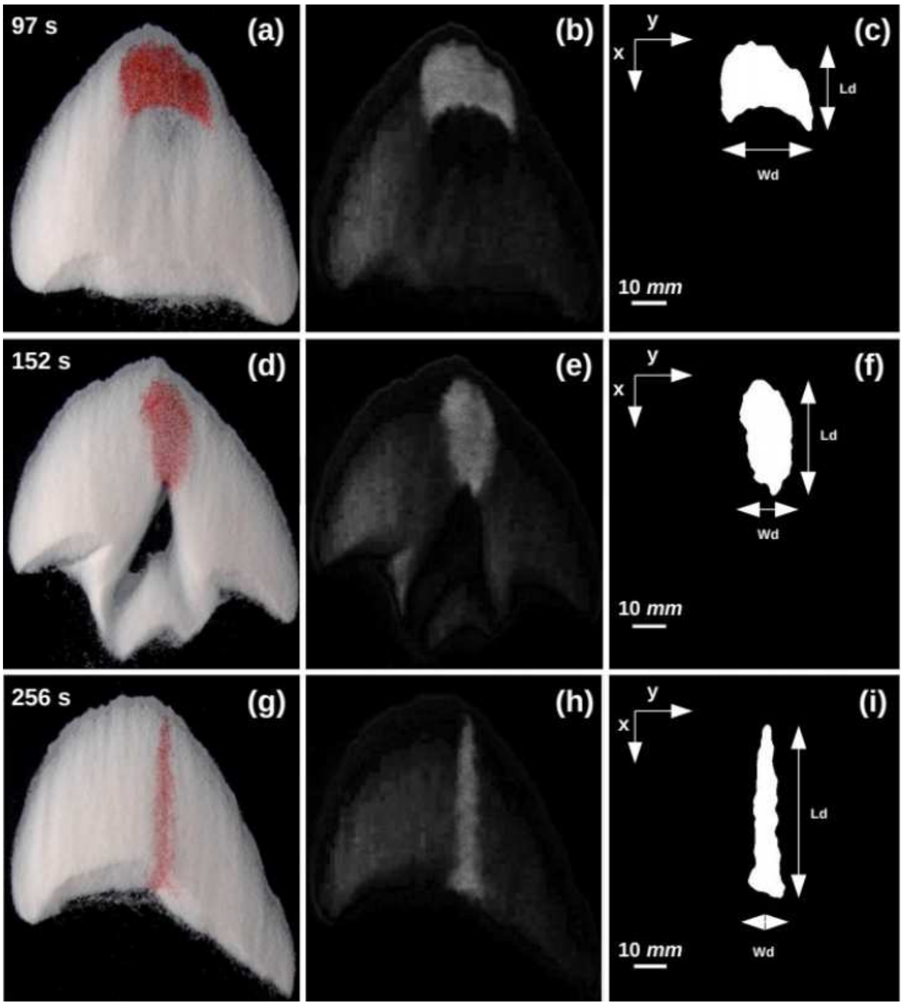

Figure 10. Distribution of grains from the impact barchan over the target one during an exchange process in the aligned case. Red (clear in figures b, e and h) grains come from the impact barchan and white (darker in figures b, e and h) grains are from the target one. From top to bottom, figures correspond to different instants (shown in figures), and from left to right figures correspond to raw, grayscale and binary images. L_d is the length and W_d the width of the structure formed with grains from the impact barchan.

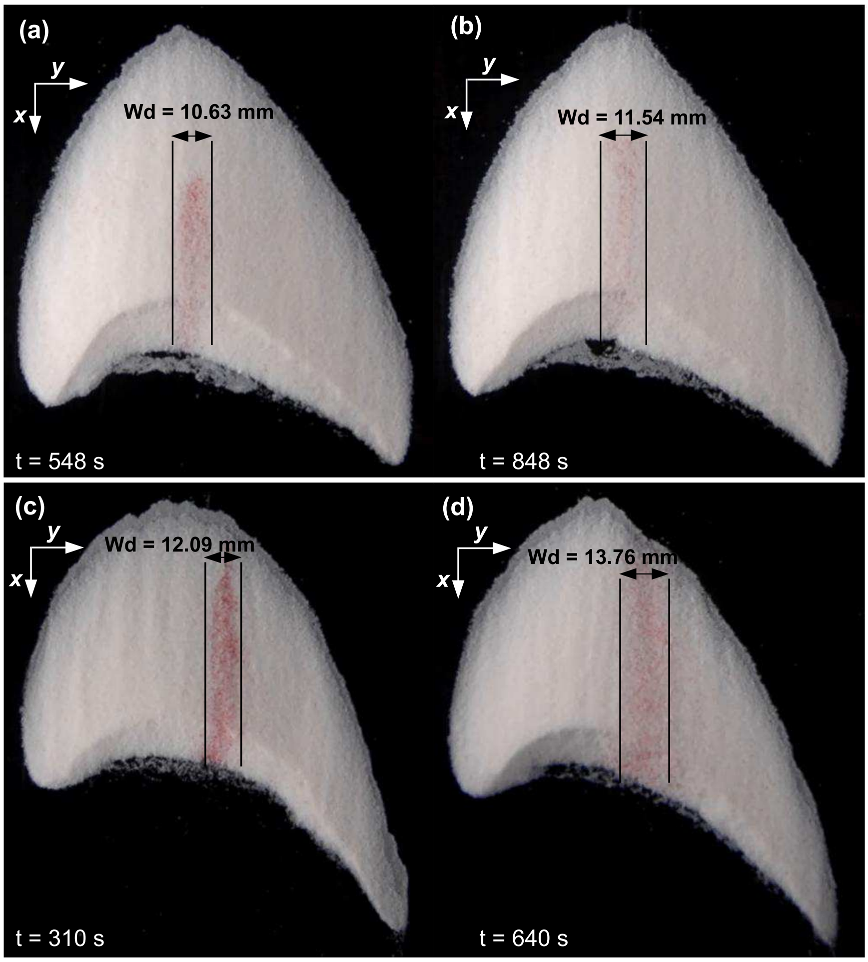

Figure 11. Second stage of the spreading of grains from the impact dune over the target one during (a) and (b) merging and (c) and (d) exchange processes. Red grains come from the impact barchan. Times and lengths are shown in the figure.

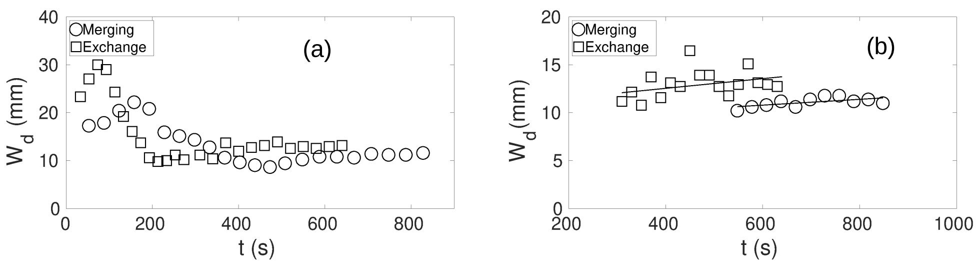

Figure 12. Width of the longitudinal stripe W_d as a function of time during (a) the entire collision processes; (b) the second stage of merging and exchange interactions. Circles and squares correspond to merging and exchange interactions, respectively, and continuous lines are linear fittings.

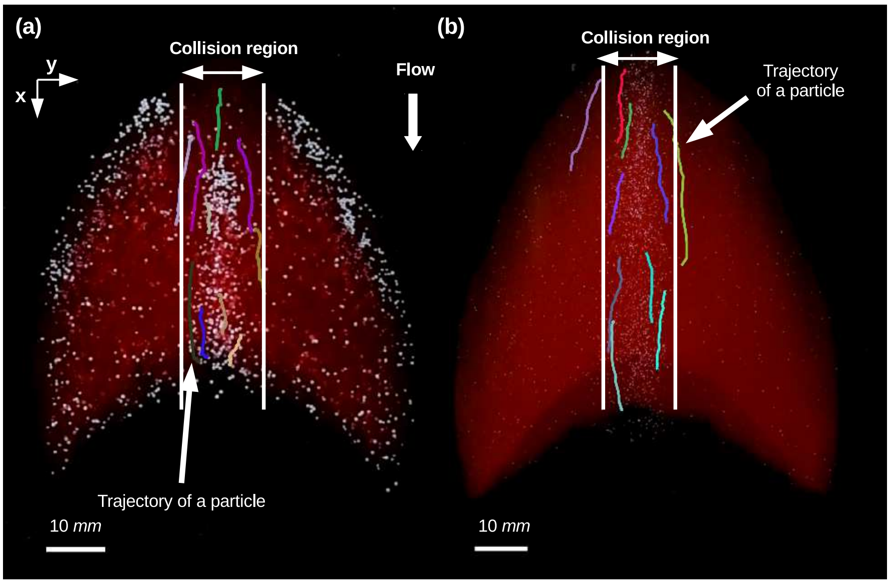

Figure 13. Typical trajectories of individual grains from the impact barchan over the target one for (a) merging and (b) exchange.

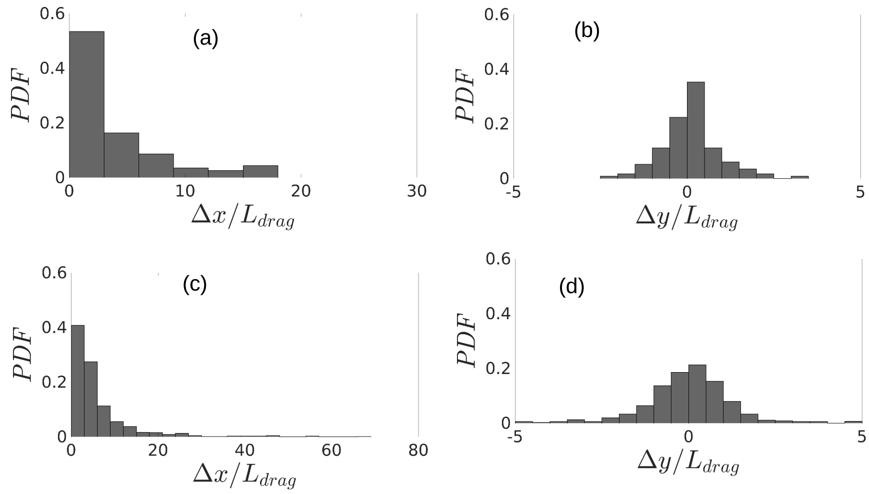

Figure 14. PDFs of total distances traveled by grains in: (a) and (c) the longitudinal direction and (b) and (d) the transverse direction, Δx and Δy, respectively, normalized by L_{drag}. Figures (a) and (b) correspond to the merging and (c) and (d) to the exchange pattern.

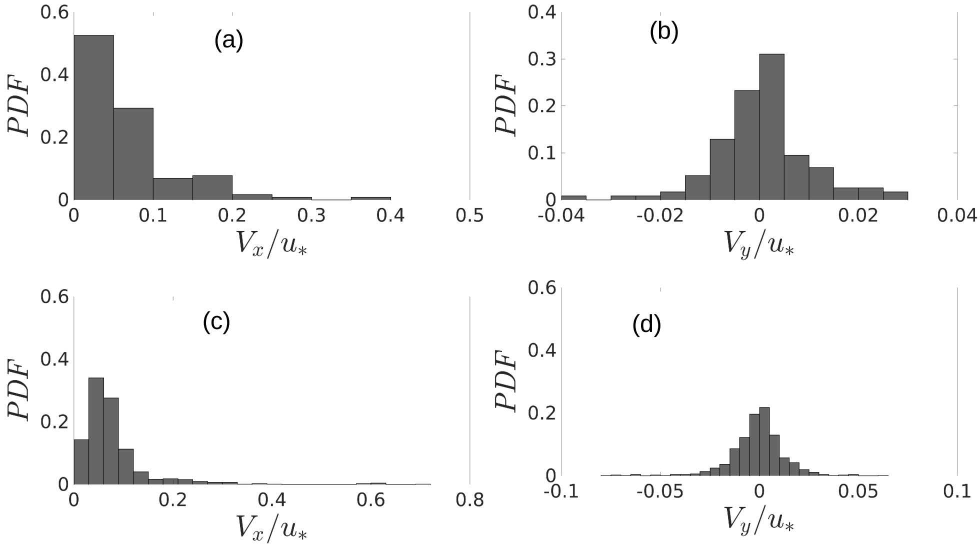

Figure 15. PDFs of time-averaged velocities in: (a) and (c) the longitudinal direction and (b) and (d) the transverse direction, V_x and V_y, respectively, normalized by u_*. Figures (a) and (b) correspond to the merging and (c) and (d) to the exchange pattern.

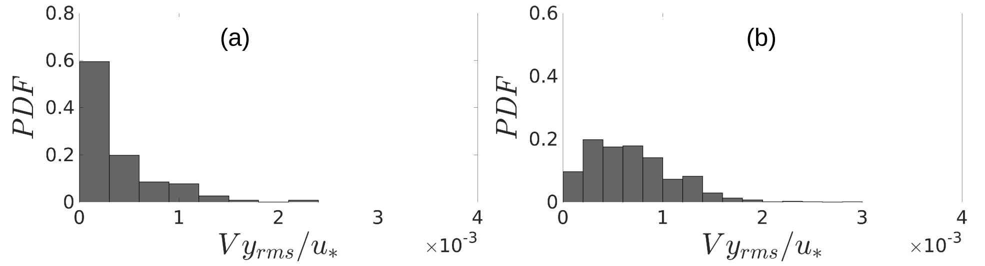

Figure 16. PDFs of the RMS average of the transverse velocity of each grain. Figure (a) corresponds to the merging and Figure (b) to the exchange pattern.

Figure 15 presents mean velocities of grains during their trajectories in the longitudinal and transverse directions, V_x (Figures 15a and 15c) and V_y (Figures 15b and 15d), respectively, normalized by u_*. Each mean value in the PDFs was computed as the time-averaged velocity of each grain during its displacement over the dune. PDFs of V_x show a decreasing distribution that is monotonic for the merging and non-monotonic for the exchange pattern. The mean velocities in the longitudinal direction are of the order of $0.1u_*$: V_x presents average values of 0.07 and $0.08u_*$, standard deviations of 0.06 and $0.08u_*$, and RMS averages of 0.09 and $0.11u_*$ for the merging and exchange patterns, respectively. PDFs of V_y are peaked close to zero, and present average values of approximately 4.0×10^{-4} and $-1.5 \times 10^{-3}u_*$, standard deviations of approximately 1.0×10^{-2} and $1.4 \times 10^{-2}u_*$, and RMS averages of 9.5×10^{-3} and $1.4 \times 10^{-2}u_*$ for the merging and exchange patterns, respectively. As for Δy, transverse velocities present an ensemble average around zero with large dispersion, indicating motions in the transverse direction that are symmetrical with respect to the longitudinal direction.

For each grain, we computed the RMS average of the transverse velocity, Vy_{rms}, during its trajectory over the barchan, and present the corresponding PDFs in Figure 16. From the PDFs, we find average values of 3×10^{-4} and $7 \times 10^{-4}u_*$ (5×10^{-6} and

11×10^{-6} m/s) for the merging and exchange cases, respectively. These values are of the same order of magnitude of those obtained for the expansion of the longitudinal stripe. PDFs of Δx, Δy, V_x, V_y and Vy_{rms} in dimensional form are available in the supporting information.

Finally, we computed the diffusion length $l_d = \sigma_y^2/(2\Delta x)$, where σ_y is the standard deviation of the transverse displacement, as proposed by Seizilles et al. (2014) for bedload over a plane bed, though in the present case grains move over a curved bed: they follow an upward slope along the symmetry line, with a varying lateral inclination from the symmetry line toward the flanks. We found $l_d/L_{drag} \approx 0.10$ and 0.20 (corresponding to $l_d/d \approx 0.3$ and $0.5d$) for the merging and exchange patterns, respectively. These values are one order of magnitude higher than that obtained by Seizilles et al. (2014), who found $l_d/L_{drag} \approx 0.012$ (or $l_d/d \approx 0.03d$). We believe that the lateral slope amplify the transverse component of the motion in subaqueous bedload, which has an erratic origin (Seizilles et al., 2014), improving significantly the transverse diffusion and increasing l_d by one order of magnitude. Because it contributes to the spreading of grains after collision has occurred, we take into consideration the slope component when computing the diffusion length.

4 Conclusions

We investigated the motion of grains while two barchans interacted with each other by performing experiments in a water channel, recording images with high-speed and conventional cameras, and tracking bedforms and individual grains along images. We found typical trajectories of grains during barchan-barchan interactions, from which we determined the origin and destination of moving grains, the proportions of grains exchanged between barchans and lost by the entire system, and the typical lengths and velocities of grains following different paths. Among our findings, we showed that the approximate deficits of granular fluxes in the aligned and off-centered configurations reach, respectively, 20 and 30% for the chasing and 60 and 20% for the fragmentation-chasing patterns. Therefore, in these patterns the downstream bedforms decrease in size, moving faster and avoiding collision with the upstream dune. Interestingly, we found that during the ejection of a new barchan in the exchange pattern in aligned configuration, 20% of grains leaving the baby barchan move toward the parent bedform, forming two granular branches that connect both dunes during a given period of time. In this particular case, we found that these grains move downstream, with mean longitudinal distances of approximately $10L_{drag}$ until reaching the parent dune and with transverse displacements of approximately $15L_{drag}$, whereas in the exchange pattern in off-centered configuration there are no grains migrating from the baby barchan toward the parent dune, the same occurring in the fragmentation exchange case (for both aligned and off-centered configurations). In addition, we followed the bedforms after collision took place in the merging and exchange patterns, revealing an initial stage, where the impact barchan is stretched until becoming a longitudinal stripe, and a second stage where the stripe widens slowly. For the second stage, we followed grains originally in the impact barchan and showed that they spread with an erratic trajectory over the target dune, having transverse velocities that scale with the front velocity of the stripe and resembling a diffusion process. For these grains, we found a diffusion length l_d of the order of $0.1L_{drag}$, one order of magnitude higher than that obtained by Seizilles et al. (2014) for subaqueous bedload over plane beds, and we conjecture that the lateral slopes of barchans amplify the transverse component of the erratic motion of grains. These results represent a step toward understanding the barchan coarsening and division, size selection, and variability of barchanoid shapes found in water, air, and other planetary environments.

Acknowledgments

W. R. Assis is grateful to FAPESP (grant no. 2019/10239-7), and E. M. Franklin is grateful to FAPESP (grant no. 2018/14981-7) and to CNPq (grant no. 400284/2016-2) for the financial support provided. The authors would like to thank Fernando David Cúñez for the assistance with the image processing code. Data supporting this work are available in the supporting information and in http://dx.doi.org/10.17632/f9p59sxm4f).

References

Andreotti, B., Claudin, P., & Douady, S. (2002). Selection of dune shapes and velocities. part 1: Dynamics of sand, wind and barchans. *Eur. Phys. J. B*, *28*, 321-329.

Assis, W. R., & Franklin, E. M. (2020). A comprehensive picture for binary interactions of subaqueous barchans. *Geophys. Res. Lett.*, *47*(18), e2020GL089464.

Bagnold, R. A. (1941). *The physics of blown sand and desert dunes.* London: Chapman and Hall.

Bo, T. L., & Zheng, X. J. (2013). Collision behaviors of barchans in aeolian dune fields. *Environ. Earth. Sci.*, *70*, 2963-2970.

Bristow, N. R., Blois, G., Best, J. L., & Christensen, K. T. (2018). Turbulent flow structure associated with collision between laterally offset, fixed-bed barchan dunes. *J. Geophys. Res.-Earth*, *123*(9), 2157-2188.

Bristow, N. R., Blois, G., Best, J. L., & Christensen, K. T. (2019). Spatial scales of turbulent flow structures associated with interacting barchan dunes. *J. Geophys. Res.-Earth*, *124*(5), 1175-1200.

Bristow, N. R., Blois, G., Best, J. L., & Christensen, K. T. (2020). Secondary flows and vortex structure associated with isolated and interacting barchan dunes. *J. Geophys. Res.-Earth*, *125*(2), e2019JF005257.

Charru, F., Andreotti, B., & Claudin, P. (2013). Sand ripples and dunes. *Ann. Rev. Fluid Mech.*, *45*(1), 469-493.

Claudin, P., & Andreotti, B. (2006). A scaling law for aeolian dunes on Mars, Venus, Earth, and for subaqueous ripples. *Earth Plan. Sci. Lett.*, *252*, 20-44.

Crocker, J. C., & Grier, D. G. (1996). Methods of digital video microscopy for colloidal studies. *Journal of Colloid and Interface Science*, *179*(1), 298-310.

Cúñez, F. D., & Franklin, E. M. (2020). Crystallization and jamming in narrow fluidized beds. *Phys. Fluids*, *32*(8), 083303.

Durán, O., Schwämmle, V., & Herrmann, H. (2005, Aug). Breeding and solitary wave behavior of dunes. *Phys. Rev. E*, *72*, 021308. Retrieved from `https://link.aps.org/doi/10.1103/PhysRevE.72.021308` doi: 10.1103/PhysRevE.72.021308

Durán, O., Schwämmle, V., Lind, P. G., & Herrmann, H. (2009). The dune size distribution and scaling relations of barchan dune fields. *Granular Matter*, *11*, 7-11.

Elbelrhiti, H., Claudin, P., & Andreotti, B. (2005). Field evidence for surface-wave-induced instability of sand dunes. *Nature*, *437*(04058).

Endo, N., Taniguchi, K., & Katsuki, A. (2004). Observation of the whole process of interaction between barchans by flume experiments. *Geophys. Res. Lett.*, *31*(12).

Gay, S. P. (1999). Observations regarding the movement of barchan sand dunes in the nazca to tanaca area of southern peru. *Geomorphology*, *27*(3), 279 - 293.

Génois, M., du Pont, S. C., Hersen, P., & Grégoire, G. (2013). An agent-based model of dune interactions produces the emergence of patterns in deserts. *Geophys. Res. Lett.*, *40*(15), 3909-3914.

Génois, M., Hersen, P., du Pont, S., & Grégoire, G. (2013). Spatial structuring and size selection as collective behaviours in an agent-based model for barchan fields. *Eur. Phys. J. B*, *86*(447).

Herrmann, H. J., & Sauermann, G. (2000). The shape of dunes. *Physica A (Amsterdam)*, *283*, 24-30.

Hersen, P. (2004). On the crescentic shape of barchan dunes. *Eur. Phys. J. B*, *37*(4), 507–514.

Hersen, P., Andersen, K. H., Elbelrhiti, H., Andreotti, B., Claudin, P., & Douady, S. (2004, Jan). Corridors of barchan dunes: Stability and size selection. *Phys. Rev. E*, *69*, 011304. Retrieved from `https://link.aps.org/doi/10.1103/PhysRevE.69.011304` doi: 10.1103/PhysRevE.69.011304

Hersen, P., & Douady, S. (2005). Collision of barchan dunes as a mechanism of size regulation. *Geophys. Res. Lett.*, *32*(21).

Hersen, P., Douady, S., & Andreotti, B. (2002, Dec). Relevant length scale of barchan dunes. *Phys. Rev. Lett.*, *89*, 264301. Retrieved from `https://link.aps.org/doi/10.1103/PhysRevLett.89.264301` doi: 10.1103/PhysRevLett.89.264301

Houssais, M., Ortiz, C. P., Durian, D. J., & Jerolmack, D. J. (2015). Onset of sediment transport is a continuous transition driven by fluid shear and granular creep. *Nat. Commun.*, *6*(6527).

Hugenholtz, C. H., & Barchyn, T. E. (2012). Real barchan dune collisions and ejections. *Geophys. Res. Lett.*, *39*(2).

Katsuki, A., Kikuchi, M., Nishimori, H., Endo, N., & Taniguchi, K. (2011). Cellular model for sand dunes with saltation, avalanche and strong erosion: collisional simulation of barchans. *Earth Surf. Process. Landforms*, *36*(3), 372-382.

Kelley, D. H., & Ouellette, N. T. (2011). Using particle tracking to measure flow instabilities in an undergraduate laboratory experiment. *Am. J. Phys.*, *79*(3), 267-273.

Kocurek, G., Ewing, R. C., & Mohrig, D. (2010). How do bedform patterns arise? new views on the role of bedform interactions within a set of boundary conditions. *Earth Surf. Process. Landforms*, *35*(1), 51-63.

Kroy, K., Sauermann, G., & Herrmann, H. J. (2002a, Sep). Minimal model for aeolian sand dunes. *Phys. Rev. E*, *66*, 031302. Retrieved from `https://link.aps.org/doi/10.1103/PhysRevE.66.031302` doi: 10.1103/PhysRevE.66.031302

Kroy, K., Sauermann, G., & Herrmann, H. J. (2002b, Jan). Minimal model for sand dunes. *Phys. Rev. Lett.*, *88*, 054301. Retrieved from `https://link.aps.org/doi/10.1103/PhysRevLett.88.054301` doi: 10.1103/PhysRevLett.88.054301

Norris, R. M., & Norris, K. S. (1961). Algodones Dunes of Southeastern California. *GSA Bulletin*, *72*(4), 605-619.

Palmer, J. A., Mejia-Alvarez, R., Best, J. L., & Christensen, K. T. (2012). Particle-image velocimetry measurements of flow over interacting barchan dunes. *Exp. Fluids*, *52*, 809-829.

Parteli, E. J. R., & Herrmann, H. J. (2007, Oct). Dune formation on the present mars. *Phys. Rev. E*, *76*, 041307. Retrieved from `https://link.aps.org/doi/10.1103/PhysRevE.76.041307` doi: 10.1103/PhysRevE.76.041307

Schlichting, H. (2000). *Boundary-layer theory.* New York: Springer.

Schwämmle, V., & Herrmann, H. J. (2003). Solitary wave behaviour of sand dunes. *Nature*, *426*, 619-620.

Schwämmle, V., & Herrmann, H. J. (2005). A model of barchan dunes including lateral shear stress. *Eur. Phys. J. E*, *16*(1), 57-65.

Seizilles, G., Lajeunesse, E., Devauchelle, O., & Bak, M. (2014). Cross-stream diffusion in bedload transport. *Phys. Fluids*, *26*(1), 013302.

Vermeesch, P. (2011). Solitary wave behavior in sand dunes observed from space. *Geophys. Res. Lett.*, *38*(22).

Zheng, X. J., Bo, T. L., & Zhu, W. (2009). A scale-coupled method for simulation of the formation and evolution of aeolian dune field. *Int. J. Nonlinear Sci. Nu-*

mer. Simul., *10*(3), 387-396.

Zhou, X., Wang, Y., & Yang, B. (2019). Three-dimensional numerical simulations of barchan dune interactions in unidirectional flow. *Particul. Sci. Technol.*, *37*(7), 835-842.